

Fluid Invasion Dynamics in Porous Media with Complex Wettability and Connectivity

Arjen Mascini^{1,2}, Marijn Boone³, Stefanie Van Offenwert^{1,2}, Shan Wang^{1,2}, Veerle Cnudde^{1,2,4} & Tom Bultreys^{1,2}

¹ Pore-scale Processes in Geomaterials Research Team (PProGRess), Department of Geology, Ghent University Krijgslaan 281/ S8, 9000 Ghent, Belgium

² Centre for X-ray Tomography (UGCT), Ghent University, Proeftuinstraat 86, 9000 Ghent, Belgium

³ TESCAN XRE, Bollebergen 2B box 1, 9052 Ghent, Belgium

⁴ Department of Earth Sciences, Utrecht University, Princetonlaan 8a, 3584 CB Utrecht, The Netherlands.

Corresponding author: Arjen Mascini (Arjen.Mascini@UGent.be)

Key points

- The pore-scale dynamics of multiphase flow in heterogeneous rocks were investigated using fast laboratory-based 4D X-ray microtomography
- We describe a pore-scale displacement mechanism with displacement rates orders of magnitude slower than those in neighboring pores
- We demonstrate that viscous forces could play a significant role even at very low global capillary numbers under mixed-wet conditions

Abstract

Multiphase flow is important for many natural and engineered processes in subsurface geoscience. Pore-scale multiphase flow dynamics are commonly characterized by an average balance of driving forces. However, significant local variability in this balance may exist inside natural, heterogeneous porous materials, such as rocks and soils. Here, we investigate multiphase flow in heterogeneous rocks with different wetting properties using fast laboratory-based 4D X-ray imaging. The mixed-wet dynamics were characterized by displacement rates that differed over orders of magnitude between directly neighboring pores. While conventional understanding predicted strongly capillary-dominated conditions, our analysis suggests that viscous forces played a key role in these dynamics, facilitated by a complex interplay between the mixed-wettability and the pore structure. These dynamics highlight the need for further studies on the fundamental controls on multiphase flow in geomaterials, which is crucial to design, e.g., groundwater remediation and subsurface CO₂ storage operations.

33 **Plain language summary**

34 The flow of multiple fluids through a porous material plays an important role in many industrial
35 and natural processes such as rain infiltrating a dry soil or CO₂ storage in the subsurface. At the
36 pore-scale, these flows are governed by forces which depend on the pore-geometry and the
37 relative affinities of the fluids with the solid (i.e. wettability). The rates at which fluids flow in
38 geological reservoirs is in most cases considered to be very slow (in the order of tens of meters
39 per year). At these slow flow rates, fluid displacements are thought to be controlled by capillary
40 forces. However, much of our current understanding of multiphase flow stems from artificial
41 samples with simplified geometries, while most natural geomaterials tend to be far more
42 complex in terms of pore structure and wettability. We show that heterogeneous pore structures
43 and wetting properties can lead to different mechanisms of fluid displacement compared to
44 those observed in model materials due to local variations in the viscous-capillary force balance.
45 This implies that models commonly used to predict subsurface flow process such as geological
46 CO₂ storage that assume capillary forces to dominate may not adequately capture the dynamics
47 at the pore-scale.

48 **1. Introduction**

49 The simultaneous flow of multiple fluid phases through a porous material is an important
50 process encountered in many natural and manmade systems. In earth sciences, it is critically
51 important for the injection and safe storage of CO₂ in deep saline aquifers (Bui et al., 2018),
52 geological energy storage (Mouli-Castillo et al., 2019) and the study of subsurface contaminant
53 transport (Mercer & Cohen, 1990).

54 The pore-scale dynamics of multiphase flow in porous media are known to be governed by a
55 competition between the driving forces on the fluids: capillary, viscous, inertial and
56 gravitational forces (Chen et al., 2019; Holtzman, 2016; Hu et al., 2019; Lenormand et al., 1983;
57 B. Zhao et al., 2016). These dynamics determine how fluids occupy the available space in the
58 pores and how the resulting fluid distribution evolves over time. Fluid invasion in 2D networks
59 was found to have qualitatively different properties when the injection flow rate or fluid
60 properties were varied (Blunt & Scher, 1995; Lenormand et al., 1988), resulting in a “phase
61 diagram” of flow regimes based on the capillary number (average ratio of viscous to capillary
62 forces) and the ratio of the viscosity of the two fluids. The development of pore-scale fluid
63 arrangements into distinct patterns has a crucial impact on the macroscopic transport behavior,
64 yet continues to challenge our pore-scale models (B. Zhao et al., 2019).

65 A particular problem has been the understanding of how pore-scale variations in the pore
66 geometry and the wettability (the relative affinity of the fluids to the solid surface) affect fluid
67 intrusion in porous materials. Recently, Lenormand's phase diagram was extended to
68 incorporate random disorder (Holtzman, 2016) and the influence of homogeneous wetting
69 conditions in 2.5D micro-models (Trojer et al., 2015; B. Zhao et al., 2016). The wettability was
70 found to strongly influence the dominant displacement mechanisms during the invasion
71 process. When the solid surfaces are non-wetting to the invading fluid (i.e., drainage)
72 displacements happen as piston-like movements associated with Haines instabilities (Haines,
73 1930; Lenormand et al., 1983). In the opposite scenario (i.e., imbibition), flow through layers
74 and corners has an important influence on the displacements (Lenormand & Zarcone, 1984). In
75 intermediate wet conditions, cooperative-pore body filling plays an important role (Cieplak &
76 Robbins, 1990).

77 Natural materials, such as porous rocks, sediments and soils, frequently exhibit much higher
78 degrees of correlated disorder than micromodels, with pore sizes spanning many orders of
79 magnitude (Blunt et al., 2013). Furthermore, the effective wettability in the pores of geological
80 materials is subject to variations in mineral composition and surface roughness at all length
81 scales (de Gennes, 1985; Morrow, 1975), and can be impacted by coatings of surface-active
82 components, particularly in hydrocarbon reservoirs (Morrow, 1990) and polluted aquifers (Al-
83 Raoush, 2009). This can lead to different surfaces having a different fluid affinity, commonly
84 referred to as "mixed-wettability" (AlRatrouf et al., 2018; Kovscek et al., 1992). The dynamics
85 in mixed-wet materials can differ from those with uniform wetting as interfaces with both
86 concave and convex shapes can co-exist while maintaining the connectivity of both fluids (Lin
87 et al., 2019; Rabbani et al., 2017). Due to structural and wetting heterogeneities, multiphase
88 flow has spatial dependencies that stretch over many pores, and consequently it is still poorly
89 understood how pore-scale heterogeneities influence the fluid invasion dynamics.

90 To study the fluid invasion dynamics in complex porous media, time-resolved high resolution
91 X-ray microtomography (mCT) can be applied to image the fluids' distribution in the pores at
92 the second to minute timescale in three dimensions (Bultreys et al., 2016; Withers et al., 2021).
93 This technique led to the first observations of capillary-dominated fluid displacement events in
94 rock samples (Berg et al., 2013; Bultreys et al., 2015; Singh et al., 2017) and of complex
95 dynamic effects, such as ganglion dynamics (Rücker et al., 2015) and intermittency (Reynolds
96 et al., 2017). Despite this significant progress, most time-resolved imaging has been performed
97 on rocks with essentially single-scale pore structures and uniform wettability. The dynamics of

98 multiphase flow in samples with a mixed-wettability, but still with a simple pore structure, have
99 only recently started to be studied (Rücker et al., 2019; Scanziani et al., 2020). Furthermore,
100 most studies have focused on describing the geometry and connectivity of the fluids during
101 displacements and in the resulting fluid distributions, while the timescales associated with the
102 dynamics received relatively little attention (Schlüter et al., 2017). This leaves unanswered
103 whether the current knowledge on capillary-dominated fluid dynamics covers the behavior that
104 typically occurs in the subsurface.

105 In this work, the pore-scale dynamics of capillary-dominated multiphase flow are investigated
106 in microcores of a heterogeneous sandstone in both homogeneously water-wet and mixed-wet
107 conditions. The timescales of fluid displacements are estimated on a pore-by-pore basis using
108 time-resolved laboratory-based X-ray mCT to image the fluid distribution in the pores. We
109 show that the dynamics were qualitatively different for mixed-wet versus water-wet conditions.
110 Under mixed-wet conditions, a significant fraction of the pores had fluid displacement
111 timescales that were several orders of magnitude slower than directly neighboring pores. These
112 slow dynamics appeared to be dominated by the fluid conductivity rather than by capillary
113 forces (despite the low capillary number). This implies that viscous forces might play an
114 important role in flow regimes commonly thought to be controlled by capillary forces. This puts
115 into question the use of classical concepts such as the capillary number to characterize
116 multiphase flow.

117 **2. Materials and methods**

118 To investigate fluid dynamics in complex porous media, we performed unsteady-state
119 multiphase flow experiments in twin microcores (29 mm long, 6 mm diameter) of a
120 heterogeneous, calcareous quarried sandstone (Luxembourg Sandstone (Molenaar, 1998)) with
121 a multiscale pore geometry (Figure 1a, S1 and S3). Mercury intrusion porosimetry showed that
122 the sample had a bimodal pore throat size distribution centered on radii $R_{\text{micro}} = \sim 2 \mu\text{m}$ and $R_{\text{inter}} = \sim 20 \mu\text{m}$
123 for the micro- and intergranular pores, respectively (Figure S1). One sample was
124 used in its native homogeneously hydrophilic state (water-wet, WW), while the wettability of
125 the second sample was chemically altered to obtain a mixed-wettability (MW) using a protocol
126 based on Herring et al. (2016). The alteration was performed by partially saturating the
127 microcore with a 5 wt.% Octadecyltrichlorosilane (OTS) solution to deposit a hydrophobic
128 coating followed by cleaning and drying the sample.

129 We performed oil- (OF) and subsequent waterflooding (WF) experiments using a $1.0 \text{ mol}\cdot\text{kg}^{-1}$
130 potassium iodide (KI) brine and n-decane, a flow rate of $0.0006 \text{ ml}/\text{min}$ and at ambient
131 temperatures. The macroscopic capillary number ($C_a = \mu v/\sigma$, where v the characteristic fluid
132 velocity in the pores, μ the invading fluid's viscosity and σ the interfacial tension) for the
133 flooding experiments was $\sim 3\cdot 10^{-8}$ using $\mu_{\text{brine}} = 0.82 \text{ mPa}\cdot\text{s}$ and $\mu_{\text{decane}} = 0.84 \text{ mPa}\cdot\text{s}$ and a σ of
134 $52 \text{ mN}\cdot\text{m}^{-1}$ (Aminabhavi et al., 1996; Gao et al., 2017; Singh et al., 2018). Under these
135 conditions, capillary forces would typically be assumed to dominate.

136 The experiments were imaged continuously using dynamic laboratory-based mCT (TESCAN
137 DynaTOM scanner) with imaging temporal resolutions of 60 seconds (WW-OF, MW-WF) and
138 120 seconds (WW-WF) per image and a voxel size of $8 \text{ }\mu\text{m}$. The dynamic imaging was
139 supplemented with higher spatial and temporal resolution imaging prior to and after each
140 experiment ($4 \text{ }\mu\text{m}/\text{vx}$ for WW and $3.5 \text{ }\mu\text{m}/\text{vx}$ for MW) was performed prior to and after each
141 flooding experiment.

142 Each reconstructed 3D image in the time series was denoised using the non-local means filter
143 (Buades et al., 2008), registered with the normalized mutual information algorithm (Studholme
144 et al., 1999) and segmented by manual thresholding in Avizo 2020.2 (Thermo Fisher Scientific)
145 to classify voxels in each image either belonging to mineral, oil or brine phase (Khishvand et
146 al., 2016; Schlüter et al., 2014).

147 To quantify the timescales of individual pore-scale displacements, the pore space was divided
148 into pore bodies separated at local constrictions using a seeded watershed algorithm on the pore
149 space distance map (PNExtract, (Raeini et al., 2017)). The fluid saturation of each pore body
150 was calculated by counting the number of segmented oil voxels within its volume at each time
151 step. The duration of a fluid displacement event (limited by the temporal resolution) was found
152 by identifying the start and finish times of the saturation change in a pore body, and calculating
153 the transient time by fitting a sigmoidal function to the normalized pore occupancy (MATLAB
154 R2018b, MathWorks) (Van Offenwert et al., 2019) (Figure 1c). Pores that changed occupancy
155 with less than 10% were omitted from the analysis to reduce the influence of image noise.
156 Contact angles were calculated using an automatic geometric method (AlRatrouf et al., 2017).

157 Further details on the materials and methods can be found in the Supporting Information.

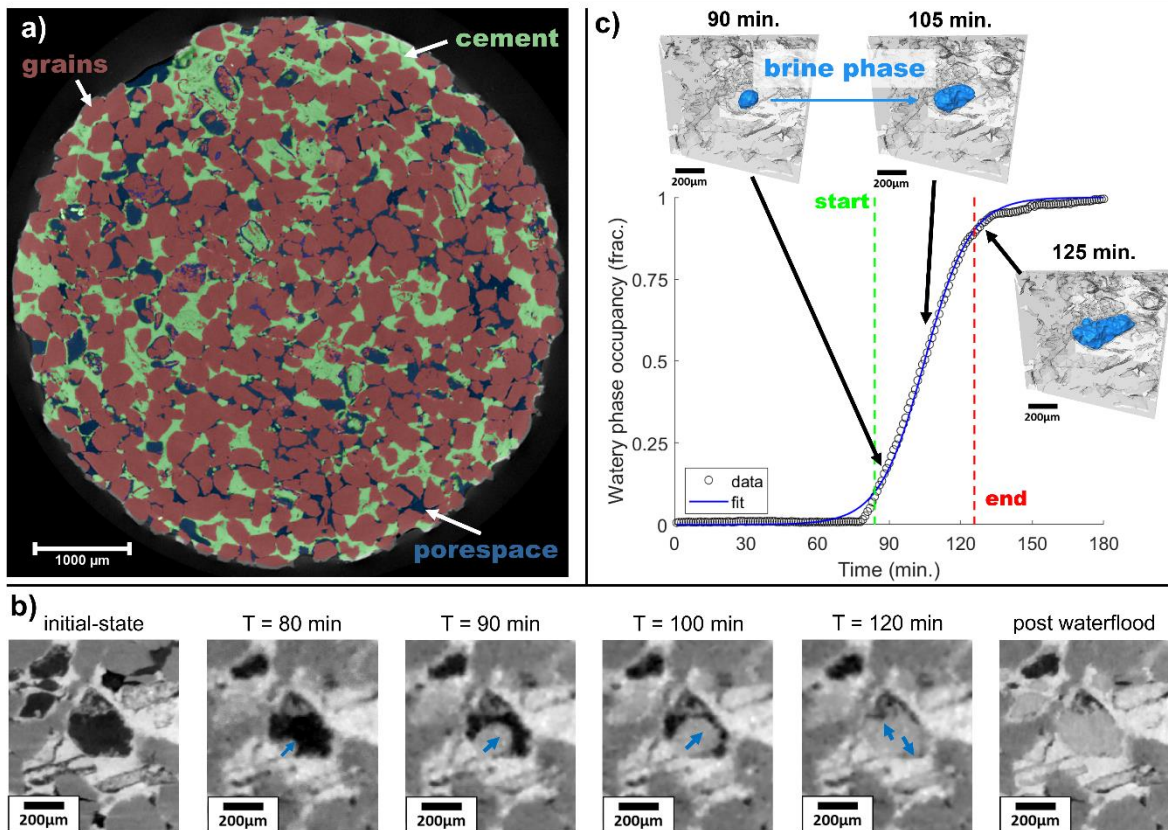
158 **3. Results and discussion**

159 Below, we first qualitatively describe our experimental results. Then, the timescales and flow
160 rates are quantified on a pore-by-pore basis. Next, the role of wettability on the displacements
161 is investigated. Finally, the viscous-capillary force balance of the observed dynamics is
162 investigated.

163 **3.1 Qualitative comparison of displacement processes**

164 Under water-wet conditions, oil was observed to displace the brine phase in a sequence of large
165 meniscus jumps (Movie S1). These jumps were significantly faster than the temporal resolution
166 of the mCT imaging, thus appearing as instantaneous pore-scale displacement events in the
167 mCT images. This conforms with the expectation that a capillary-dominated drainage process
168 takes place as an intermittent sequence of Haines jumps at the milli-second timescale
169 (Armstrong & Berg, 2013). In the subsequent waterflooding experiment (Movie S2), water
170 layers were observed to slowly swell from the sides of the pores (Figure S6), causing the oil to
171 become disconnected by the occurrence of sudden snap-off events in narrow constrictions of
172 the pore space. This is typical behavior for slow imbibition in a water-wet medium with a high
173 pore-throat aspect ratio (Singh et al., 2019), and led to significant trapping of the oil-phase.

174 The sample with a mixed-wettability showed a notably different behavior during waterflooding
175 (Figure 1b; Movie S3). The majority of the displacements were filled in fast events comparable
176 to the drainage process in the water-wet sample. However, three observations stood out. First,
177 the front at which the displacements occurred was more compact than that of the water-wet
178 drainage case (Figure S7). Second, a significant part of the pores changed fluid occupancy over
179 a much slower timescale: it took tens of minutes rather than a single time step for a fluid
180 meniscus to move through such a pore. The slow events occurred concurrently with the fast
181 events in neighboring pores. These slow events typically happened in poorly connected moldic
182 pores, that often appear to be only connected to the rest of the network by micropores below
183 the imaging resolution. Third, the pore walls of many of these pores visually appeared to be
184 partly water-wet and partly oil-wet (Figure 1b). We observed both events where brine moved
185 into the center of the pore body while bulging into the oil (Figure 1b; Movie S4-5) and events
186 with a near flat meniscus (Figure S6; Movie S6-7). This was distinct from layer swelling during
187 waterflooding of the water-wet sample, where the water-layers always swelled from the smaller
188 pores and corners.



189

190 *Figure 1 a) 2D slice through the tomogram of the initial-state image of the MW sample with in colors the segmented phases.*
 191 *b) Visual comparison of a “slow” events show different fluid configurations of water (light grey) and oil (black). The blue*
 192 *arrows indicate the movement of the brine phase. Note that the brine phase bulges into the oil-phase indicating oil-wet*
 193 *conditions. c) By calculating the fluid occupancy over time for a single pore body, displacements can be identified and the*
 194 *duration of the event calculated.*

195 3.2 Quantification of pore-scale displacements events

196 In this section, the timescales of the displacement events are quantified to relate them to the
 197 overall flow conditions and characteristics of the sample.

198 In the water-wet sample, 98% of the displaced volume during the oilflood was associated with
 199 pore filling events that completed faster than the temporal resolution of the imaging (Figure
 200 2a). Longer pore filling events were associated with two or more intermittent displacements
 201 inside one pore body that each took less than one time step to complete. Displacements during
 202 the waterflood in the same sample took typically 10-20 min to complete. Note that the filling
 203 duration calculated here included the reversible swelling of wetting layers, which led up to
 204 capillary instabilities and subsequent “snap-off” redistributions of the fluids.

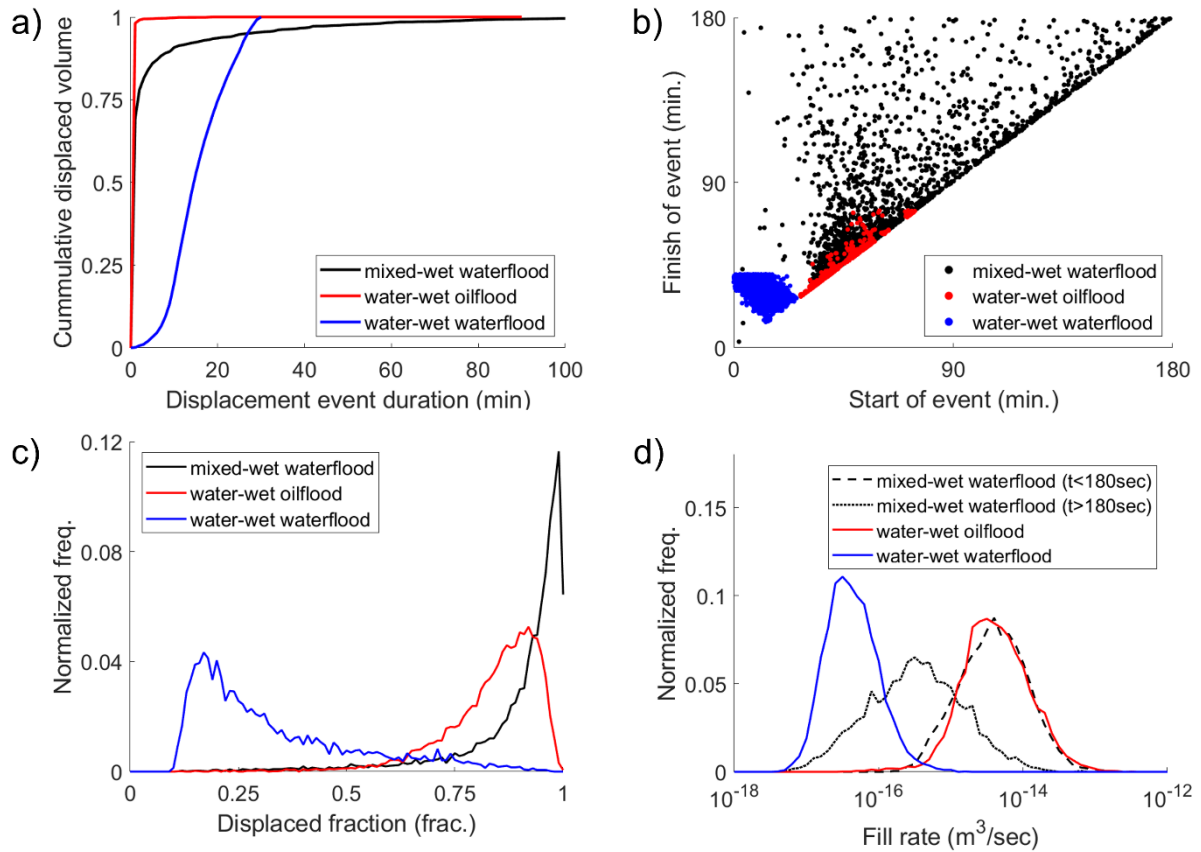
205 The displacements in the MW-WF case had a distinctively different temporal signature. While
 206 most of the fluid displacement occurred in events that took less than one time step to complete,
 207 19% of the displaced oil volume was associated with events that took longer than 60 seconds.

208 The cumulative pore filling duration distribution shown in Figure 2a has a long tail, spanning
209 almost the full duration of the experiment. These slow fillings appeared not to be dominated by
210 capillary forces in the same way as during a typical drainage, which would have resulted in
211 instabilities that caused fast fluid redistribution as soon as the invasion capillary pressure of a
212 pore throat was overcome. On average, the slow displacement events took place in pores with
213 lower connectivity than the instantaneous events: only 46% of the former (filling time >10
214 minutes) had at least one connection to the percolating cluster of resolved macro-pores,
215 compared to 80% of the latter. Displacements with a long duration occurred concurrently with
216 those that completed within one time step (Figure 2b), which shows the start and finish time of
217 each detected displacement event. The slow filling dynamics may thus have a non-trivial
218 influence on the order in which pores are invaded by brine, and therefore potentially on the
219 fluid distribution patterns that arise from this (Figure S9).

220 The waterflooding process under mixed-wet conditions was found to be able to displace a larger
221 fraction of the volume of a pore body than the drainage process in the WW sample (Figure 2c)
222 highlighting the importance of the role of surface wetting on the overall displacement processes.
223 It also clearly shows the distinction between the slow events in the water-wet waterflooding
224 (due to layer swelling) and the slow invasion events in the mixed-wet waterflooding, which
225 tended to invade the pore centers in a piston-like manner. Moreover, this may affect the energy
226 balance of the displacement process due to differences in energy dissipation between the
227 different displacement processes.

228 The rate at which fluids flow through a porous medium is closely related to the capillary-viscous
229 force balance that control the fluid distributions. We define the effective displacement rate as
230 the volume of displaced fluid within a pore divided by the duration of this displacement. The
231 calculated effective displacement rates are shown in Figure 2d. These are a lower limit to the
232 actual displacement rates due to the limited temporal resolution of the measurement. Note that
233 the effective filling rates for a single pore were up to six orders of magnitude slower than the
234 overall flow rate set on the pump ($1 \cdot 10^{-11} \text{ m}^3/\text{sec}$).

235



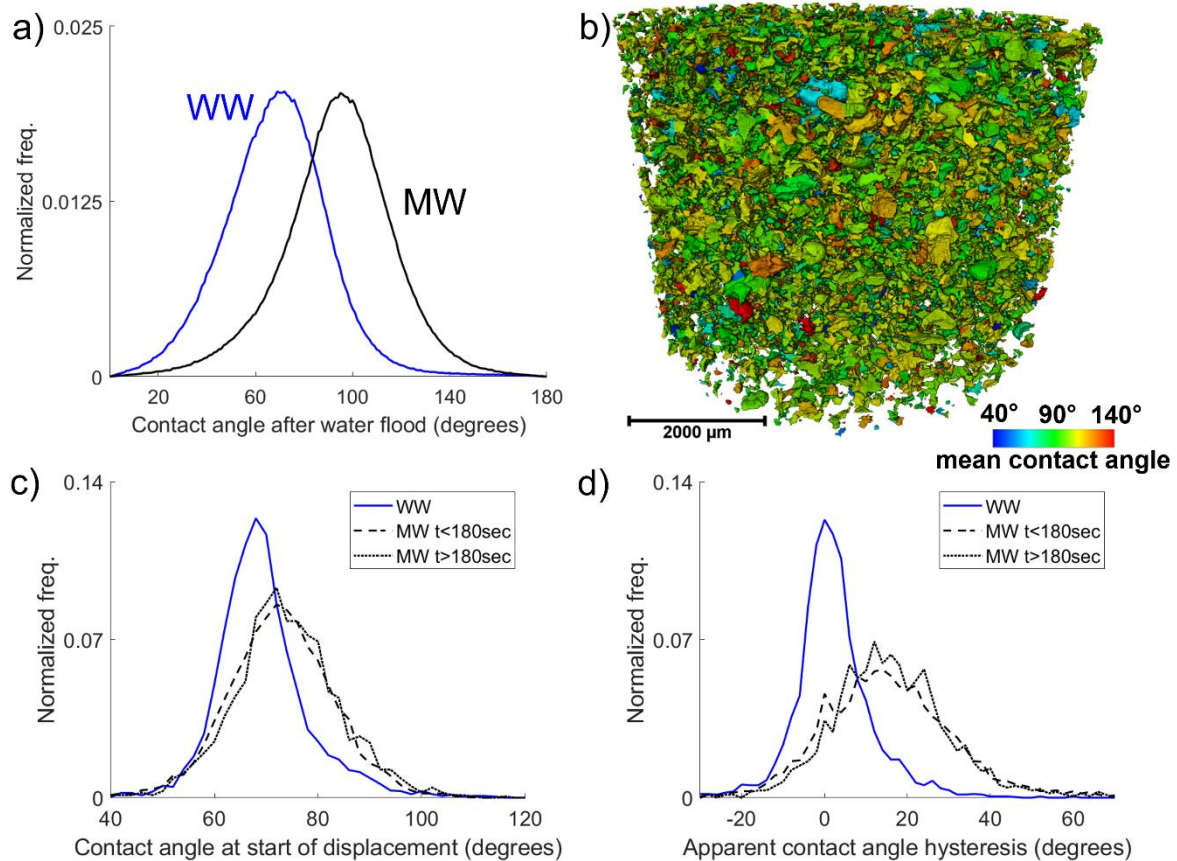
236

237 *Figure 2 a) During the waterflood in the MW sample more than 19% of the total displaced volume of fluid occurred in events*
 238 *that took more than a minute to complete. b) Start and finish times were identified on a pore-by-pore basis. c) Waterflooding*
 239 *displacements under MW conditions were able to displace a substantial larger amount of defending phase within a pore body*
 240 *compared to the imbibition and drainage processes observed under WW conditions. d) Distribution of effective fill rates for*
 241 *fluid displacement events in individual pores. The calculated effective rate or events occurring faster than the temporal*
 242 *resolution is a lower limit and is likely much higher. For MW conditions, events with a duration shorter than 180 seconds are*
 243 *plotted separately from those who took more than 180 seconds to complete.*

244 3.3 Wettability and pore scale dynamics

245 Wettability has a strong influence on the position of the fluid-fluid interfaces during multiphase
 246 flow and can alter the sequence in which pores are invaded in mixed-wet media (Scanziani et
 247 al., 2020). The wettability of a material is quantified by a contact angle, that can be calculated
 248 geometrically directly from 3D mCT images of fluid distributions (AIRatrou et al., 2017).
 249 Contact angles were calculated on high-resolution images of the static fluid distributions after
 250 waterflooding and are presented in Figure 3 for both samples. The mean contact angle
 251 calculated for the sample in its native state suggested weakly water-wet conditions (69°). The
 252 pore-by-pore mean contact angle varied through the pore space for the MW sample (Figure 3b),
 253 with part of the distribution below and above 90° (mean of 94°). While these contact angle
 254 distributions likely carry significant uncertainty due to the limited spatial resolution, high levels
 255 of image noise, and (to a lesser extent) due to fluid meniscus dynamics (Akai et al., 2019;
 256 Mascini et al., 2020; Sun et al., 2020), the observed shift between the distributions in the two

257 samples indicated a shift to mixed-wet conditions in the OTS-treated sample (AlRatrou et al.,
 258 2018).



259

260 *Figure 3 a) Distributions of contact angles on static fluid distributions after the waterflood. The mixed-wet distribution shows*
 261 *a distribution that covers both values above and below 90 degrees which is typical for mixed-wet rocks. b) The spatial*
 262 *distribution of contact angles post waterflood averaged for each pore body inside the mixed-wet sample. c) Distribution of the*
 263 *mean contact angles for each pore body at the start of the displacement event calculated on the dynamic mCT data of the water-*
 264 *and mixed-wet data. d) Distribution of the apparent contact angle hysteresis per pore for both water- and mixed-wet conditions*
 265 *during waterflooding. In both c) and d) there is no obvious difference in distribution between events that take less than 180*
 266 *seconds and events that take longer to complete.*

267 By themselves, the measured wettability properties of the mixed-wet sample did not explain
 268 the slow filling dynamics that we observed. In addition to the “static” contact angles in Figure
 269 3a, we investigated the relation between the wettability and the dynamics by measuring the
 270 local contact angles at the start of each fluid invasion event in the dynamic imaging data
 271 (Mascini et al., 2020). Unlike contact angle measurements on static fluid distributions, which
 272 contain pinned contact lines that can yield any value between the advancing and receding
 273 contact angles, the latter “event-based” measurements indicate the contact angle at the time
 274 when fluid displacements started (Figure 3c). In our mixed-wet experiment, the event-based
 275 contact angles were very similar in fast- and slow-filling pores, as was the hysteresis between
 276 the measured contact angles at the start and end of the filling events (Figure 3d). This suggests

277 that the time-scale of the dynamics was not controlled by the local wettability alone.
278 Nevertheless, contact angle measurements on fast time resolved mCT data may suffer from the
279 limited spatial and temporal resolution of these measurements. Further experiments at
280 synchrotron facilities which offer imaging capabilities at higher resolutions are needed to
281 confirm this.

282 **3.4 Filling dynamics and the viscous-capillary force balance**

283 In the capillary limit, fluid displacement can only take place if both fluid phases are connected
284 through the sample (i.e. there is no mobilization of trapped ganglia due to viscous forces). When
285 connected fluid pathways become narrow, the area available for fluid flow may limit the rate
286 of fluid displacements. Conductivity-limited behavior has been observed indirectly during the
287 final stages of drainage experiments in water-wet rocks (El-Maghraby & Blunt, 2013). During
288 these final stages, the water phase is displaced via a network of thin water layers in the corners
289 and crevices of rough pore walls. As the area available for the water phase is limited, the relative
290 permeability is very low (orders of magnitude lower than the relative permeability of the non-
291 wetting phase). The time it takes to reach capillary equilibrium in this case can be days for a
292 small cm-scale sample, compared to the timescale of milliseconds of the initial Haines jumps
293 that filled most of the pore space (Blunt, 2017). There are, however, important differences with
294 the fluid filling events described in this work: (1) the events occur concurrently with the fast
295 displacements in neighboring pores and (2) the events fill complete pore bodies rather than
296 consisting of interfaces merely invading small pore corners and crevices. As such, the slow
297 events have the potential of severely impacting the displacement sequence, and thus fluid
298 connectivity and the resulting upscaled flow properties.

299 The prevalence of the slow filling events can be explained by taking into account both the
300 wettability and the pore space architecture. Microporous materials, such as mineral cements
301 and clays, can provide structural bottle necks between larger intergranular pores that impede
302 fluid flow. The pore throats in these narrow structures might differ orders of magnitude with
303 larger neighboring pores. Large heterogeneity in the pore size promotes the loss of fluid
304 connectivity during the invasion, due to trapping by, e.g., snap-off and bypassing (Blunt, 2017).
305 However, mixed-wet systems are known to preserve this connectivity longer than
306 homogeneously-wetted systems (Lin et al., 2019; J. Zhao et al., 2018). As a consequence, filling
307 events that cannot proceed in a water-wet systems, may proceed in mixed-wet systems. When
308 this happens, narrow connections through micro-pores and wetting layers therein may cause
309 bottlenecks in the fluids' "supply chain", thereby causing conductance-limited behavior that

310 significantly slows down the pore-scale invasion dynamics. This likely explains why slow
 311 filling dynamics were less pronounced in previous studies of mixed-wet systems with simpler
 312 pore structures, such as Bentheimer sandstone or Ketton limestone (Rücker et al., 2019;
 313 Scanziani et al., 2020).

314 The local balance between viscous and capillary forces during the slow filling events can be
 315 investigated using a simple model of the pore space architecture in our experiment. We model
 316 the situation that the invading fluid had to pass through a patch of tight throat radii to invade a
 317 large pore. The flow thus passed through an intergranular pore (throat) with typical dimensions
 318 on the order of $R_{inter} \times R_{inter} \times R_{inter}$ (20 μ m), which was cemented with microporous material
 319 with throat size R_{micro} (2 μ m). Using respectively the multiphase extension of the Darcy equation
 320 and the Young-Laplace equation, the balance between the viscous pressure drop P_v over this
 321 blocked throat and its capillary intrusion pressure P_c is:

$$322 \quad \frac{P_v}{P_c} = \frac{\mu q_{local} R_{inter}}{k_{micro} \cdot k_{micro,r}} \cdot \frac{R_{micro}}{2\sigma |\cos \theta|} = Ca_{local} \cdot \frac{R_{micro} \cdot R_{inter}}{k_{micro} \cdot k_{micro,r}} \cdot \frac{1}{2 |\cos \theta|}$$

323 Where μ is viscosity, q_{local} is the local fluid flux approximated by the effective displacement
 324 rate, k_{micro} and $k_{micro,r}$ are the absolute and relative permeability of the microporosity, σ is the
 325 interfacial tension, θ is the advancing contact angle and Ca_{local} is a local capillary number
 326 defined to equal $\mu q_{local} / \sigma$. Following (Blunt, 2017), a typical permeability for the microporosity
 327 with this throat size is on the order of 10^{-15} m^2 , and an average contact angle of 94° (Figure 3a,
 328 assuming a similar contact angle for the micropores). Using these values, we find that:

$$329 \quad \frac{P_v}{P_c} \approx 10^5 \cdot \frac{Ca_{local}}{k_{m,r}}$$

330 Based on the flow rates measured in the mCT data, the typical Ca_{local} for slow pore filling
 331 events mediated by this microporous patch would be on the order of 10^{-7} (Figure S8). Given the
 332 fact that the relative permeability to either the invading or the escaping phase is expected to be
 333 low ($\ll 10^{-1}$) in a mixed-wet medium, the local ratio between viscous and capillary forces can
 334 easily approach values on the order of 1. This indicates that in samples where pore sizes differ
 335 orders of magnitude, viscous forces could play a significant role in the displacement process
 336 even at very low global capillary numbers. The mixed-wet wettability plays a crucial role here,
 337 as it allows to maintain fluid connectivity – and thus displacement processes to proceed – even
 338 for very low relative permeabilities to either of the fluids (Lin et al. 2019). Further imaging
 339 studies at higher resolutions are needed to confirm this.

340 **4. Conclusions**

341 One of the main open questions in the field of multiphase flow is how to link pore-scale
342 displacements to macro-scale behavior of multiphase flow. As the underlying pore-scale
343 displacement dynamics in water-wet and mixed-wet conditions are poorly understood, we used
344 time-resolved microcomputed tomography to image unsteady-state multiphase flow
345 experiments in a calcareous sandstone with a complex pore structure. The pore-scale dynamics
346 were qualitatively and quantitative different for water- and mixed-wet conditions.
347 Displacements during the oil-flood in the water wet-sample were associated with Haines
348 instabilities, while corner and layer flow with subsequent snap-offs were observed during the
349 water-flood of this sample. In the waterflooding of a mixed-wet sample, we identified a
350 displacement mechanism during which 19% of the displaced volume was associated with
351 displacements took longer than 60 seconds to complete. The slow displacement events occur
352 concurrently with Haines instabilities occurring in directly neighboring pores and are
353 characterized by the fluid meniscus moving through the center of the pore space.

354 The occurrence of viscous effects has been demonstrated experimentally for higher capillary
355 numbers (10^{-6} - 10^{-4}), in the form of intermittency (Reynolds et al., 2017), ganglion dynamics
356 (Rücker et al., 2015) or break-up of ganglia in rocks with a multiscale pore system (Pak et al.,
357 2015). The work presented here demonstrates that even at much lower capillary numbers ($\sim 10^{-8}$),
358 pore-scale complexities, such as mixed-wettability and multi-scale pore geometries, can
359 cause significant pore-scale variations in the capillary-viscous force balance. This can influence
360 the displacement process in complex pore spaces, particularly under mixed-wet conditions.
361 Therefore, such effects need to be considered when performing pore network modeling of
362 multiphase flow in complex pore spaces. Our observations spur further investigation into the
363 classification of phenomena caused by pore-scale variability in the driving forces of multiphase
364 flow in heterogeneous porous materials. Ultimately, this may lead to better models of fluid flow
365 in the subsurface critical for groundwater resources and CO₂ sequestration operations.

366 **Acknowledgements**

367 We would like to thank TESCAN XRE for the access to their DynaTOM system and their
368 support during the experiments. Sorin Pop, Carina Bringedal and Stephan Lunowa are thanked
369 for their insightful discussions that helped to give shape to this work. This research received
370 funding from the Research Foundation–Flanders (FWO, project G051418N). Tom Bultreys is

371 a postdoctoral fellow of the Research Foundation–Flanders (FWO) and acknowledges its
372 support under grant 12X0919N.

373 **Data Availability Statement**

374 The data described in this manuscript can be retrieved from
375 <https://doi.org/10.17612/GEN3-2P41>.

376 **References**

- 377 Akai, T., Lin, Q., Alhosani, A., Bijeljic, B., & Blunt, M. (2019). Quantification of Uncertainty and
378 Best Practice in Computing Interfacial Curvature from Complex Pore Space Images.
379 *Materials*, 12(13), 2138. <https://doi.org/10.3390/ma12132138>
- 380 Al-Raoush, R. I. (2009). Impact of Wettability on Pore-Scale Characteristics of Residual Nonaqueous
381 Phase Liquids. *Environmental Science & Technology*, 43(13), 4796–4801.
382 <https://doi.org/10.1021/es802566s>
- 383 AlRatrou, A., Raeini, A. Q., Bijeljic, B., & Blunt, M. J. (2017). Automatic measurement of contact
384 angle in pore-space images. *Advances in Water Resources*, 109, 158–169.
385 <https://doi.org/10.1016/j.advwatres.2017.07.018>
- 386 AlRatrou, A., Blunt, M. J., & Bijeljic, B. (2018). Wettability in complex porous materials, the mixed-
387 wet state, and its relationship to surface roughness. *Proceedings of the National Academy of*
388 *Sciences*, 201803734. <https://doi.org/10.1073/pnas.1803734115>
- 389 Aminabhavi, T. M., Patil, V. B., Aralaguppi, M. I., & Phayde, H. T. S. (1996). Density, Viscosity, and
390 Refractive Index of the Binary Mixtures of Cyclohexane with Hexane, Heptane, Octane,
391 Nonane, and Decane at (298.15, 303.15, and 308.15) K. *Journal of Chemical & Engineering*
392 *Data*, 41(3), 521–525. <https://doi.org/10.1021/je950279c>
- 393 Armstrong, R. T., & Berg, S. (2013). Interfacial velocities and capillary pressure gradients during
394 Haines jumps. *Physical Review E*, 88(4), 043010.
- 395 Berg, S., Ott, H., Klapp, S. A., Schwing, A., Neiteler, R., Brussee, N., et al. (2013). Real-time 3D
396 imaging of Haines jumps in porous media flow. *Proceedings of the National Academy of*
397 *Sciences*, 110(10), 3755–3759. <https://doi.org/10.1073/pnas.1221373110>
- 398 Blunt, Martin J., & Scher, H. (1995). Pore-level modeling of wetting. *Physical Review E*, 52(6), 6387–
399 6403. <https://doi.org/10.1103/PhysRevE.52.6387>
- 400 Blunt, Martin J., Bijeljic, B., Dong, H., Gharbi, O., Iglauer, S., Mostaghimi, P., et al. (2013). Pore-
401 scale imaging and modelling. *Advances in Water Resources*, 51, 197–216.
402 <https://doi.org/10.1016/j.advwatres.2012.03.003>
- 403 Blunt, M.J. (2017). *Multiphase Flow in Permeable Media: A Pore-Scale Perspective*. Cambridge
404 University Press. Retrieved from <https://books.google.be/books?id=G1kHDgAAQBAJ>
- 405 Buades, A., Coll, B., & Morel, J.-M. (2008). Nonlocal Image and Movie Denoising. *International*
406 *Journal of Computer Vision*, 76(2), 123–139. <https://doi.org/10.1007/s11263-007-0052-1>
- 407 Bui, M., Adjiman, C. S., Bardow, A., Anthony, E. J., Boston, A., Brown, S., et al. (2018). Carbon
408 capture and storage (CCS): the way forward. *Energy & Environmental Science*, 11(5), 1062–
409 1176. <https://doi.org/10.1039/C7EE02342A>
- 410 Bultreys, T., Boone, M. A., Boone, M. N., De Schryver, T., Masschaele, B., Van Loo, D., et al.
411 (2015). Real-time visualization of Haines jumps in sandstone with laboratory-based
412 microcomputed tomography. *Water Resources Research*, 51(10), 8668–8676.
413 <https://doi.org/10.1002/2015WR017502>
- 414 Bultreys, T., Boone, M. A., Boone, M. N., De Schryver, T., Masschaele, B., Van Hoorebeke, L., &
415 Cnudde, V. (2016). Fast laboratory-based micro-computed tomography for pore-scale
416 research: Illustrative experiments and perspectives on the future. *Advances in Water*
417 *Resources*, 95, 341–351. <https://doi.org/10.1016/j.advwatres.2015.05.012>
- 418 Chen, Y., Valocchi, A. J., Kang, Q., & Viswanathan, H. S. (2019). Inertial Effects During the Process
419 of Supercritical CO₂ Displacing Brine in a Sandstone: Lattice Boltzmann Simulations Based

- 420 on the Continuum-Surface-Force and Geometrical Wetting Models. *Water Resources*
 421 *Research*, 55(12), 11144–11165. <https://doi.org/10.1029/2019WR025746>
- 422 Cieplak, M., & Robbins, M. O. (1990). Influence of contact angle on quasistatic fluid invasion of
 423 porous media. *Physical Review B*, 41(16), 11508–11521.
 424 <https://doi.org/10.1103/PhysRevB.41.11508>
- 425 El-Maghraby, R. M., & Blunt, M. J. (2013). Residual CO₂ Trapping in Indiana Limestone.
 426 *Environmental Science & Technology*, 47(1), 227–233. <https://doi.org/10.1021/es304166u>
- 427 Gao, Y., Lin, Q., Bijeljic, B., & Blunt, M. J. (2017). X-ray Microtomography of Intermittency in
 428 Multiphase Flow at Steady State Using a Differential Imaging Method. *Water Resources*
 429 *Research*, 53(12), 10274–10292. <https://doi.org/10.1002/2017WR021736>
- 430 de Gennes, P. G. (1985). Wetting: statics and dynamics. *Reviews of Modern Physics*, 57(3), 827–863.
 431 <https://doi.org/10.1103/RevModPhys.57.827>
- 432 Haines, W. B. (1930). Studies in the physical properties of soil. V. The hysteresis effect in capillary
 433 properties, and the modes of moisture distribution associated therewith. *The Journal of*
 434 *Agricultural Science*, 20(1), 97–116.
- 435 Herring, A. L., Sheppard, A., Andersson, L., & Wildenschild, D. (2016). Impact of wettability
 436 alteration on 3D nonwetting phase trapping and transport. *International Journal of*
 437 *Greenhouse Gas Control*, 46, 175–186. <https://doi.org/10.1016/j.ijggc.2015.12.026>
- 438 Holtzman, R. (2016). Effects of Pore-Scale Disorder on Fluid Displacement in Partially-Wettable
 439 Porous Media. *Scientific Reports*, 6(1), 36221. <https://doi.org/10.1038/srep36221>
- 440 Hu, R., Lan, T., Wei, G.-J., & Chen, Y.-F. (2019). Phase diagram of quasi-static immiscible
 441 displacement in disordered porous media. *Journal of Fluid Mechanics*, 875, 448–475.
 442 <https://doi.org/10.1017/jfm.2019.504>
- 443 Khishvand, M., Alizadeh, A. H., & Piri, M. (2016). In-situ characterization of wettability and pore-
 444 scale displacements during two- and three-phase flow in natural porous media. *Advances in*
 445 *Water Resources*, 97, 279–298. <https://doi.org/10.1016/j.advwatres.2016.10.009>
- 446 Kovscek, A. R., Wong, H., & Radke, C. J. (1992). A Pore-Level Scenario for the Development of
 447 Mixed-Wettability in Oil Reservoirs. *AIChE J Journal*, 39(1072–1085), 58.
- 448 Lenormand, R., & Zarcone, C. (1984). Role of roughness and edges during imbibition in square
 449 capillaries. *SPE Journal*, (13264).
- 450 Lenormand, R., Zarcone, C., & Sarr, A. (1983). Mechanisms of the displacement of one fluid by
 451 another in a network of capillary ducts. *Journal of Fluid Mechanics*, (135), 337–353.
- 452 Lenormand, R., Touboul, E., & Zarcone, C. (1988). Numerical models and experiments on immiscible
 453 displacements on immiscible displacements in porous media. *Journal of Fluid Mechanics*,
 454 (189), 165–187.
- 455 Lin, Q., Bijeljic, B., Berg, S., Pini, R., Blunt, M. J., & Krevor, S. (2019). Minimal surfaces in porous
 456 media: Pore-scale imaging of multiphase flow in an altered-wettability Bentheimer sandstone.
 457 *Physical Review E*, 99(6), 063105. <https://doi.org/10.1103/PhysRevE.99.063105>
- 458 Mascini, A., Cnudde, V., & Bultreys, T. (2020). Event-based contact angle measurements inside
 459 porous media using time-resolved micro-computed tomography. *Journal of Colloid and*
 460 *Interface Science*, 572, 354–363. <https://doi.org/10.1016/j.jcis.2020.03.099>
- 461 Mercer, J. W., & Cohen, R. M. (1990). A review of immiscible fluids in the subsurface: Properties,
 462 models, characterization and remediation. *Journal of Contaminant Hydrology*, 6(2), 107–163.
 463 [https://doi.org/10.1016/0169-7722\(90\)90043-G](https://doi.org/10.1016/0169-7722(90)90043-G)
- 464 Molenaar, N. (1998). Origin of Low-Permeability Calcite-Cemented Lenses in Shallow Marine
 465 Sandstones and CaCO₃ Cementation Mechanisms: An Example from the Lower Jurassic
 466 Luxemburg Sandstone, Luxemburg. In S. Morad (Ed.), *Carbonate Cementation in Sandstones*
 467 (pp. 193–211). Oxford, UK: Blackwell Publishing Ltd.
 468 <https://doi.org/10.1002/9781444304893.ch9>
- 469 Morrow, N. R. (1975). The Effects of Surface Roughness On Contact: Angle With Special Reference
 470 to Petroleum Recovery. *Journal of Canadian Petroleum Technology*, 14(04).
 471 <https://doi.org/10.2118/75-04-04>
- 472 Morrow, N. R. (1990). Wettability and Its Effect on Oil Recovery. *Journal of Petroleum Technology*,
 473 42(12), 1–476.

- 474 Mouli-Castillo, J., Wilkinson, M., Mignard, D., McDermott, C., Haszeldine, R. S., & Shipton, Z. K.
 475 (2019). Inter-seasonal compressed-air energy storage using saline aquifers. *Nature Energy*,
 476 4(2), 131–139. <https://doi.org/10.1038/s41560-018-0311-0>
- 477 Pak, T., Butler, I. B., Geiger, S., van Dijke, M. I. J., & Sorbie, K. S. (2015). Droplet fragmentation: 3D
 478 imaging of a previously unidentified pore-scale process during multiphase flow in porous
 479 media. *Proceedings of the National Academy of Sciences*, 112(7), 1947–1952.
 480 <https://doi.org/10.1073/pnas.1420202112>
- 481 Rabbani, H. S., Joekar-Niasar, V., Pak, T., & Shokri, N. (2017). New insights on the complex
 482 dynamics of two-phase flow in porous media under intermediate-wet conditions. *Scientific*
 483 *Reports*, 7(1), 4584. <https://doi.org/10.1038/s41598-017-04545-4>
- 484 Raeini, A. Q., Bijeljic, B., & Blunt, M. J. (2017). Generalized network modeling: Network extraction
 485 as a coarse-scale discretization of the void space of porous media. *Physical Review E*, 96(1).
 486 <https://doi.org/10.1103/PhysRevE.96.013312>
- 487 Reynolds, C. A., Menke, H., Andrew, M., Blunt, M. J., & Krevor, S. (2017). Dynamic fluid
 488 connectivity during steady-state multiphase flow in a sandstone. *Proceedings of the National*
 489 *Academy of Sciences*, 114(31), 8187–8192. <https://doi.org/10.1073/pnas.1702834114>
- 490 Rucker, M., Berg, S., Armstrong, R. T., Georgiadis, A., Ott, H., Schwing, A., et al. (2015). From
 491 connected pathway flow to ganglion dynamics. *Geophysical Research Letters*, 42(10), 3888–
 492 3894. <https://doi.org/10.1002/2015GL064007>
- 493 Rucker, M., Bartels, W. -B., Singh, K., Brussee, N., Coorn, A., Linde, H. A., et al. (2019). The Effect
 494 of Mixed Wettability on Pore-Scale Flow Regimes Based on a Flooding Experiment in Ketton
 495 Limestone. *Geophysical Research Letters*, 46(6), 3225–3234.
 496 <https://doi.org/10.1029/2018GL081784>
- 497 Scanziani, A., Lin, Q., Alhosani, A., Blunt, M. J., & Bijeljic, B. (2020). *Dynamics of displacement in*
 498 *mixed-wet porous media* (preprint). EarthArXiv. <https://doi.org/10.31223/osf.io/jpmvc>
- 499 Schlüter, S., Sheppard, A., Brown, K., & Wildenschild, D. (2014). Image processing of multiphase
 500 images obtained via X-ray microtomography: A review. *Water Resources Research*, 50(4),
 501 3615–3639. <https://doi.org/10.1002/2014WR015256>
- 502 Schlüter, S., Berg, S., Li, T., Vogel, H.-J., & Wildenschild, D. (2017). Time scales of relaxation
 503 dynamics during transient conditions in two-phase flow: RELAXATION DYNAMICS. *Water*
 504 *Resources Research*, 53(6), 4709–4724. <https://doi.org/10.1002/2016WR019815>
- 505 Singh, K., Menke, H., Andrew, M., Lin, Q., Rau, C., Blunt, M. J., & Bijeljic, B. (2017). Dynamics of
 506 snap-off and pore-filling events during two-phase fluid flow in permeable media. *Scientific*
 507 *Reports*, 7(1). <https://doi.org/10.1038/s41598-017-05204-4>
- 508 Singh, K., Menke, H., Andrew, M., Rau, C., Bijeljic, B., & Blunt, M. J. (2018). Time-resolved
 509 synchrotron X-ray micro-tomography datasets of drainage and imbibition in carbonate rocks.
 510 *Scientific Data*, 5(1). <https://doi.org/10.1038/sdata.2018.265>
- 511 Singh, K., Bultreys, T., Raeini, A. Q., Shams, M., & Blunt, M. J. (2019). Imbibition in porous media:
 512 correlations of displacement events with pore-throat geometry and the identification of a new
 513 type of pore snap-off, 12. <https://doi.org/10.31223/osf.io/62gfr>
- 514 Studholme, C., Hill, D. L., & Hawkes, D. J. (1999). An overlap invariant entropy measure of 3D
 515 medical image alignment. *Pattern Recognition*, 32(1), 71–86.
- 516 Sun, C., McClure, J. E., Mostaghimi, P., Herring, A. L., Meisenheimer, D. E., Wildenschild, D., et al.
 517 (2020). Characterization of wetting using topological principles. *Journal of Colloid and*
 518 *Interface Science*, 578, 106–115. <https://doi.org/10.1016/j.jcis.2020.05.076>
- 519 Trojer, M., Szulczewski, M. L., & Juanes, R. (2015). Stabilizing Fluid-Fluid Displacements in Porous
 520 Media Through Wettability Alteration. *Physical Review Applied*, 3(5), 054008.
 521 <https://doi.org/10.1103/PhysRevApplied.3.054008>
- 522 Van Offenwert, S., Cnudde, V., & Bultreys, T. (2019). Pore-Scale Visualization and Quantification of
 523 Transient Solute Transport Using Fast Microcomputed Tomography. *Water Resources*
 524 *Research*, 55(11), 9279–9291. <https://doi.org/10.1029/2019WR025880>
- 525 Withers, P. J., Bouman, C., Carmignato, S., Cnudde, V., Grimaldi, D., Hagen, C. K., et al. (2021). X-
 526 ray computed tomography. *Nature Reviews Methods Primers*, 1(1), 18.
 527 <https://doi.org/10.1038/s43586-021-00015-4>

- 528 Zhao, B., MacMinn, C. W., & Juanes, R. (2016). Wettability control on multiphase flow in patterned
529 microfluidics. *Proceedings of the National Academy of Sciences*, *113*(37), 10251–10256.
530 <https://doi.org/10.1073/pnas.1603387113>
- 531 Zhao, B., MacMinn, C. W., Primkulov, B. K., Chen, Y., Valocchi, A. J., Zhao, J., et al. (2019).
532 Comprehensive comparison of pore-scale models for multiphase flow in porous media.
533 *Proceedings of the National Academy of Sciences*, *116*(28), 13799–13806.
534 <https://doi.org/10.1073/pnas.1901619116>
- 535 Zhao, J., Kang, Q., Yao, J., Viswanathan, H., Pawar, R., Zhang, L., & Sun, H. (2018). The Effect of
536 Wettability Heterogeneity on Relative Permeability of Two-Phase Flow in Porous Media: A
537 Lattice Boltzmann Study. *Water Resources Research*, *54*(2), 1295–1311.
538 <https://doi.org/10.1002/2017WR021443>
539